Limnol. Oceanogr., 55(3), 2010, 1271–1288

doi:10.4319/lo.2010.55.3.1271

Remineralization of upper ocean particles: Implications for iron biogeochemistry

P. W. Boyd,[a,*] E. Ibisanmi,[b] S. G. Sander,[b] K. A. Hunter,[b] and G. A. Jackson[c]

[a] National Institute of Water and Atmosphere Centre of Chemical and Physical Oceanography, Department of Chemistry, University of Otago, Dunedin, New Zealand

[b] Department of Chemistry, University of Otago, Dunedin, New Zealand

[c] Department of Oceanography, Texas A&M University, College Station, Texas

Abstract

The role of heterotrophic bacteria in iron recycling, the influence of complexation on iron remineralization, and iron mobilization rates from lithogenic vs. biogenic particulate iron (PFe) were examined using field experiments and modeling simulations. During summer, we measured the mobilization rate of algal iron by heterotrophic bacteria in the mixed layer at a polar and a subpolar site south of Australia, and conducted shipboard incubations to track the release of dissolved iron (DFe) and iron-binding ligands from subsurface settling particles sampled from 120-m depth. Bacteria mobilized $> 25\%$ PFe d^{-1} in surface waters relative to mobilization at depth ($< 2\%$ d^{-1}). Our incubations provide the first evidence of the concurrent release of weak iron-binding ligands and DFe from sinking particles. Simulated profiles of PFe remineralization, based on proxies, point to greater dissolution from biogenic PFe than from lithogenic PFe. Together our findings point to different biogeochemical functions for lithogenic vs. biogenic PFe: biogenic PFe is probably the main source of both DFe and ligands, whereas lithogenic PFe may contribute most to DFe scavenging and ballasting of biogenic PFe. The relative proportions of lithogenic vs. biogenic PFe flux vary regionally and set the contribution of scavenging and ballasting vs. dissolution and ligand release, and hence the fate of iron in the water column.

Over the last two decades the role of iron supply on the ocean's carbon cycle has received widespread attention because of its potential function in modulating the earth's climate during the geological past (Martin 1990). Such attention has resulted in rapid advances in this field, with the development of distinct research themes including iron and algal physiology (Morel and Price 2003), iron chemistry (Rue and Bruland 1995), dissolved iron (DFe) distributions and oceanic circulation (Bergquist and Boyle 2006), mesoscale iron enrichments and their biogeochemical and ecological effects (Boyd 2004), iron biogeochemistry and dust supply (Duce and Tindale 1991), and iron biogeochemical modeling (Johnson et al. 1997; Parekh et al. 2004). Together, they enable a better understanding of the oceanic biogeochemical cycle of iron. Much of this body of research has focused on sources of new iron such as dust (Duce and Tindale 1991; Moore and Braucher 2008). Thus, comparatively little attention has been directed recently on what controls the supply of regenerated iron (Bruland et al. 1991; Hutchins and Bruland 1994), even though it dominates iron supply in high-nitrate low-chlorophyll (HNLC) waters, which are characterized by *f*e ratios of < 0.1 (*f*e = new Fe/[new Fe + regenerated Fe]; Boyd et al. 2005).

Particles form the largest iron pool in the upper ocean, but to date have received disproportionately little research effort from the iron chemistry and biogeochemistry communities (Moffett 2002; Frew et al. 2006; Lamborg et al. 2008). The mobilization rate of particulate iron (PFe) sets both its short-term cycling (hours to days) in the surface mixed layer, and its longer-term fate (weeks to months) in the underlying waters. Pelagic recycling influences the rate of iron resupply to upper ocean biota (Barbeau et al. 1996, 2001*a*; Strzepek et al. 2005), whereas the dissolution of PFe at depth represents a major unknown in modeling iron biogeochemistry, for example in simulations of ocean iron fertilization (Gnanadesikan et al. 2003). Gnanadesikan et al. (2003) conclude that model simulations of the iron-mediated drawdown of atmospheric carbon dioxide are particularly sensitive to the representation of PFe remineralization and the long-term fate of the iron. Remineralization is not simply about the conversion of PFe to DFe; another major factor, about which little is known, is whether iron-binding ligands are also released and/or produced during the process (Hunter and Boyd 2007). One putative source of iron-binding ligands during remineralization is cellular debris (Hutchins et al. 1999), which may play a key role in maintaining this remineralized iron in the dissolved phase in the subsurface ocean (Rue and Bruland 1997; Hunter and Boyd 2007).

Previous studies of PFe recycling in the surface mixed layer, often termed the "ferrous wheel" (Kirchman 1996), point to the important role of both grazers, such as mesozooplankton (Hutchins and Bruland 1994) and microzooplankton (Barbeau et al. 1996; Strzepek et al. 2005), and heterotrophic bacteria (Sarthou et al. 2008) in controlling the rate of PFe turnover. Furthermore, in sunlit surface waters, the influence of photochemistry on iron bioavailability, the fate of strong iron-binding ligands (Barbeau et al. 2001*b*; Barbeau 2006), and photodissolution of algal detritus (Mayer et al. 2009) has important ramifications for rates of iron mobilization. Few studies have investigated the mobilization of iron in the underlying waters. In this stratum, there has been little attenuation in the downward flux of PFe with depth in subsurface HNLC waters of the southwest (upper 150 m) and northwest

* Corresponding author: Pboyd@alkali.otago.ac.nz

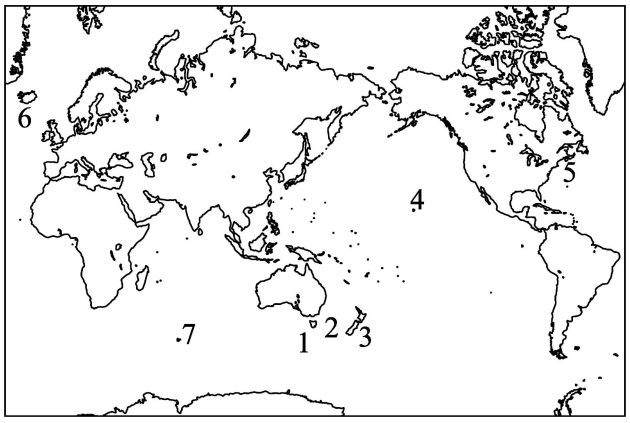

Fig. 1. Map showing the locations of both study sites (1 denotes PFZ; 2, NSAZ), along with the locales used in the modeling simulations (3 denotes FeCycle; 4, ALOHA; 5, BATS; 6, NABE). Our findings were mainly compared with two other Southern Ocean sites—FeCycle and KEOPS (denoted by 7).

(upper 500 m) Pacific, respectively (Frew et al. 2006; Lamborg et al. 2008). In contrast, there was greater attenuation of the downward particulate organic carbon (POC) flux at these sites, suggesting lower rates of remineralization for PFe in the subsurface ocean (Frew et al. 2006; Lamborg et al. 2008). This difference in PFe and POC cycling in deeper waters contrasts with the rapid recycling of both PFe and POC reported for the upper ocean (Barbeau et al. 2001*a*; Strzepek et al. 2005; Sarthou et al. 2008). Frew et al. (2006) reported indirect evidence of transformations of lithogenic PFe to biogenic PFe within the upper 100 m of the water column at this HNLC FeCycle site (Fig. 1), suggesting that treating PFe as a bulk property or flux may hinder our understanding of its biogeochemical role in the iron cycle.

To obtain a clearer picture of the biogeochemical role of transformations of PFe in both surface and subsurface waters, we addressed three questions, the first two by shipboard experiments and the third by model simulations. First, what are the timescales and rate of algal iron mobilization by heterotrophic bacteria in the mixed layer? Second, are weak iron-binding ligands also produced during the remineralization of PFe to DFe in subsurface waters? Third, how does the differential remineralization of the three main components of the downward PFe flux (lithogenic, detrital, and algal) contribute to the mobilization of iron and the resulting DFe inventory? The main findings, used to address these questions, were then brought together to develop an improved conceptual model of the role particle remineralization on iron biogeochemistry.

Methods

Two sites were sampled in Southern Ocean waters south of Tasmania, Australia, during austral summer from the research vessel *Aurora Australis* as part of the Sub-Antarctic Zone: Sensitivity to Environmental Change (SAZ-SENSE) voyage. Polar waters at a site (54.04°S, 146.25°E) just south of the polar frontal zone (PFZ) were sampled in January and February 2007, and the waters of the northern subantarctic zone (NSAZ) at 45.46°S, 153.29°E were sampled in mid-February 2007 (Fig. 1). Additional background information on SAZ-SENSE is in Bowie et al. (2009).

Heterotrophic bacterial mobilization of algal iron—The goal of our experiments was to investigate the mobilization rates of radiolabeled Fe subsequent to its uptake by natural phytoplankton assemblages (cells > 5 μm) using the transfer of radiolabel between different size classes as a means to detect mobilization to particles < 5 μm (i.e., heterotrophs) and/or into the dissolved phase (Fig. 2), using a time series of dark incubations. We adapted the design and rationale of Bidle and Azam (1999), who incubated radioactively labeled (^{14}C and ^{32}Si) marine diatom cultures in order to follow the relative remineralization rates of Si vs. C by heterotrophic bacteria.

At the PFZ and SAZ sites, seawater was collected using trace metal–clean protocols from within both the seasonal mixed layer (20-m depth) and the deep chlorophyll maxima (DCMs, around 40-m depth at each site) on 02 February 2007 (PFZ) and 11 February 2007 (SAZ). We collected samples using a General Oceanics model 1018 autonomous intelligent rosette specially modified for trace metal work, with 12 $\times$ 5-liter Niskin-1010X Teflon-lined (externally closing) bottles attached to Kevlar line. Samples from each depth were transferred to 15 replicate trace metal–clean 500-mL polycarbonate bottles, spiked with ^{55}Fe ($FeCl_3$, specific activity of 89.81 mCi mg^{-1}, Aldrich) that was added as 2 nmol L^{-1} Fe : 10 μmol L^{-1} ethylenediaminetetraacetic acid to mimic the low Fe′ in HNLC regions (Maldonado and Price 1999). These were incubated in a simulated in situ deckboard incubator for 24 h at an environmentally appropriate percentage of incident irradiance (I_o) for the surface mixed layer (i.e., 25% I_o) and DCM (i.e., 2% I_o) using neutral-density polycarbonate screening.

After this incubation, the contents of each bottle were passed under gravity through a trace metal–clean 47-mm-diameter 5-μm-porosity polycarbonate filter and the filtrate discarded (Fig. 2). After triple-rinsing with < 0.2-μm seawater, three of the filters were prepared for scintillation counting after McKay et al. (2005) to provide initial estimates of iron uptake by cells > 5 μm. Immediately after filtration, the remaining filters were resuspended in 50 mL of trace metal–clean < 1.0-μm seawater. Then, the suspended cells (mainly phytoplankton but with the likelihood of some larger heterotrophs) were added to trace metal–clean 500-mL polycarbonate bottles. The vessels contained either 0.2-μm-filtered seawater ($<$ 50–mm Hg vacuum), to assess abiotic mobilization of Fe (Bidle and Azam 1999), or < 1.0-μm-filtered seawater ($<$ 40–mm Hg vacuum) to follow the role of heterotrophic bacteria in mobilizing the Fe (Fig. 2).

Each bottle was double-wrapped in aluminum foil (as the incubation required the absence of light to unambiguously follow the mobilization of the ^{55}Fe-labeled phytoplankton) and incubated in a simulated in situ deckboard

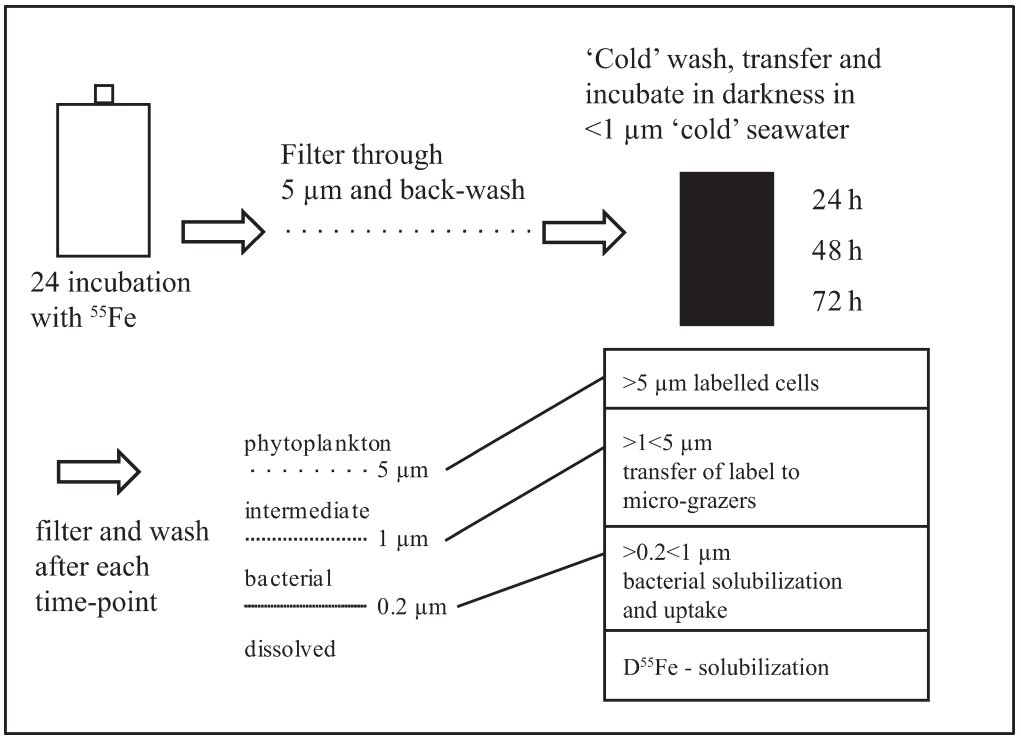

Fig. 2. Schematic of the experimental procedure used to radiolabel phytoplankton cells, the transfer of the labeled cells, and tracking of the mobilization of the radiolabeled iron into various size classes. The interpretation of the subsequent size partitioning of label is presented in the lower right of this figure, but *see* main text for other possible interpretations. We could not distinguish between intracellular and extracellularly bound iron at the start of our experiment as all available iron washes, such as oxalate or titanium, are toxic.

incubator for up to 72 h. Samples were not collected until after 24 h had elapsed to ensure bacterial colonization of the phytoplankton (Bidle and Azam 1999). Three replicate bottles, containing the < 1-μm filtrate, were harvested after 24, 48, and 72 h incubation through a filter cascade containing 5-, 1-, and 0.2-μm-porosity 47-mm-diameter polycarbonate filters in series (Fig. 2). We designate material retained on these filters as the algal, intermediate, and bacterial size fractions. An aliquot of the 0.2-μm filtrate was also retained to measure the activity of ^{55}DFe. Three replicate bottles, containing both labeled particles and $<$ 0.2-μm filtrate, were filtered in a similar manner after 48 h to examine the influence of abiotic activity on Fe mobilization. Each filter was prepared for scintillation counting after McKay et al. (2005) to assess the size partitioning of the labeled iron. The design of these experiments relied upon some assumptions regarding what the size partitioning of the labeled iron represented (*see* Fig. 2 caption); however, the presence of labeled iron within the $>$ 1-μm $<$ 5-μm fraction could also be due to the growth of gammaproteobacteria (Cho et al. 2007) over the 48–72 h incubations, and/or disintegration of $>$ 5-μm cells or detritus during gravity filtration.

Release of iron and iron-binding ligands from mesopelagic particles—Particles $>$ 53 μm were also collected at each of the PFZ and NSAZ stations using in situ pumps (McLane Research Laboratories) fitted with an acid-leached, 142 mm-diameter, 54-μm-porosity polyester filter (Sefar Filtration). At the PFZ site, 809 liters of seawater was filtered at 122-m depth (mixed-layer depth was 40 m) on 03 February 2007, and at the NSAZ site 828 liters of seawater was pumped through the filter at 115-m depth (mixed-layer depth was 25 m) on 13 February 2007. The collected particles were resuspended immediately upon recovery of the pumps in 100 mL trace metal–clean seawater previously sampled from 125-m depth, under class 100 conditions, prior to incubation of the particles.

Seawater (12 liters) for the incubations was collected from 125-m depth from both the PFZ and NSAZ sites 24 h prior to each pump deployment using the trace metal–clean rosette. The water was kept refrigerated (4°C) overnight. For the incubations, 3 liters of this unfiltered seawater was used as control and divided into 10 $\times$ 250-mL subsamples. The resuspended particles from the filter were transferred to the remaining 9 liters of seawater from the station and gently agitated to homogenize the suspension. This particle-enriched (around 90-fold greater than ambient, i.e., 9 liters vs. 809 liters; 9 liters vs. 828 liters) suspension was subdivided into 30 $\times$ 250-mL subsamples; 10 of these subsamples were heat-sterilized using a household microwave (15 min at 1000 W). The control samples, the sterilized samples, and 10 of the particle-enriched untreated samples were incubated in the dark for up to 12 d (i.e., the final time point) at 4°C for PFZ and for up to 5 d at 8°C for NSAZ. Ten samples from each station were incubated at elevated temperatures of 8°C and 15°C, to investigate whether temperature would stimulate greater heterotrophic

activity on the particles for the two sites. The lower incubation temperatures were the ambient temperatures at 122-m and 115-m depth at the PFZ and NSAZ sites.

At each time point in the incubation, samples were filtered under gentle vacuum (< 50 mm Hg) through a 0.2-μm-porosity polycarbonate 47-mm-diameter filter using a trace metal–clean polycarbonate filter apparatus (Sartorius). The filtrate for ligand and DFe measurements was collected by filling acid-cleaned 500-mL polyethylene bottles. They were double-bagged, stored at -20°C, transported frozen to the lab, and thawed immediately prior to analysis. Trace metal–clean techniques were used throughout this study.

Analysis of the ligands and total DFe—Iron-complexing ligands were determined by competitive ligand exchange adsorptive cathodic stripping voltammetry (CLE-ACSV; Croot and Johansson 2000; Ibisanmi et al. in press). The voltammetric equipment consisted of a Metrohm VA 663 stand including a multimode electrode. The system was connected via the IME 663 interface to a μAutolab type III potentiostat (both Eco Chemie). The working electrode was a hanging mercury drop electrode with a mercury drop size 2 (0.4 mm^2 $\pm$ 10%), the reference electrode was Ag|AgCl|3 mol L^{-1} KCl, and the counter electrode was a glassy carbon rod. All samples were contained in Teflon cells (Metrohm) during ACSV analysis and stirred with the inbuilt all-polytetrafluoroethylene (Teflon) stirring tip (at 1500 rotations per minute [rpm]) of the VA 663. For the Fe-ligand titration, subsamples (12 mL) of seawater were pipetted into a series of 14 Teflon bottles and buffered at pH 8.0 with 50 μL of 1.0 mol L^{-1} buffer solution of *N*-(2-hydroxyethyl)-piperazine-*N*′-2-propanesulfonic acid (EPPS; Sigma-Aldrich).

Iron was added to 12 of the bottles, yielding concentrations from 0.2 to 6 nmol L^{-1}. The added Fe was allowed to equilibrate with the natural ligands for 30–60 min at room temperature. After this equilibration period, 2-(2-thiazolylazo)-p-cresol (TAC) was added to the bottles to a final concentration of 3.5 μmol L^{-1}, and the sample was left to equilibrate for at least 8 h (often overnight, 15–18 h). The equilibrated solutions were transferred to the Teflon cell cup for analysis in order of total Fe concentration. Each solution was deaerated for 3 min with oxygen-free nitrogen gas. A fresh Hg drop was made, and Fe(TAC)$_2$ complex species were adsorbed at an applied potential of -0.4 V for 120 s, while stirring at 1500 rpm. The stirrer was switched off for a 5-s quiescent period. Then, the potential was scanned in the differential pulse mode (potential step = 2.55 mV, pulse amplitude = 49.95 mV) from -0.38 to -0.60 V and the cathodic stripping current was recorded. The peak current I_p from the reduction of iron in the Fe(TAC) complex appears under these parameters at -0.458 ± 0.005 V. Cell cups were rinsed with Milli-Q water between different concentrations within one titration analysis. The cell and electrodes were additionally rinsed with acid between titrations. Specific Teflon bottles were always used for the same iron concentration added and they were rinsed only with either Milli-Q or the sample itself in between titrations to maintain equilibrium.

The theory of CLE-ACSV using TAC is detailed in Croot and Johansson (2000). All speciation data for K'_{FeL} and L values were calculated using the Gerringa nonlinear regression (Gerringa et al. 1995). Classification of ligand classes (i.e., strong ligands, L1, and the sum of all ligands, ΣL, representing a weighted average of all of the ligands present) was done using the approach detailed in Ibisanmi et al. (in press). In brief, $\log K'_{FeL1,Fe3+}$ is defined as > 22 (i.e., a measure of the relative binding strength of the ligand complex specific for seawater), and log $K_{Fe\Sigma L,Fe3+}$ represents all ligands within the detection window. In the absence of L1, $\sum$L can be assumed to represent only the weaker ligand class. We have here defined L2 as the weaker ligand that may be produced via remineralization. The standard deviations of K'_{FeL} and L were calculated using nonlinear least squares regression of the titration curves with the computer program NLREG (www.nlreg.com). Errors were reported for 95% confidence intervals.

DFe samples that had been acidified to pH 2 were UV digested for 6 h using a Photoreactor Model APQ 40 (Photochemical Reactors) with a 400-W medium-pressure Hg lamp. The pH of the samples was brought back to pH 8.0 with isothermally distilled NH_4OH prior to analysis using the ACSV protocols (as described above). DFe concentrations in the samples were determined using the method of standard additions, and the total reagent blank including HNO_3, NH_4OH, EPPS, and TAC was 0.15 ± 0.01 nmol L^{-1} ($n = 3$).

Modeling PFe downward export and remineralization—The modeling approach explores how representing the downward PFe flux as each of its three main components—lithogenic (aerosol or laterally transported), biogenic (detrital, heterogeneous particles or aggregates), and biogenic (algal aggregates)—as opposed to a bulk PFe flux might enhance our understanding of the role of export and remineralization within the iron biogeochemical cycle. As no published data are available on the vertical attenuance of the PFe flux of each of these components, we had to rely on proxies for each. Because of the paucity of data, we chose a relatively simple one-dimensional water column model. We used datasets from the sole site—ALOHA in the north subtropical Pacific gyre (Fig. 1; Lamborg et al. 2008)—that has sufficient data coverage to provide vertical attenuation coefficients for POC (i.e., a proxy for detrital iron), chlorophyll (i.e., a proxy for algal iron), and PFe (i.e., a proxy for lithogenic iron) downward fluxes.

The model assumes that DFe is released during the remineralization of iron from downward fluxes of three forms of PFe—lithogenic (inorganic) iron (F_L), detrital iron (F_D), and algal iron (F_A). Attenuation of the flux with depth increases the concentration C of DFe at a rate of

$$\frac{\partial C}{\partial t} = -\frac{\partial F}{\partial z}$$

In addition, vertical mixing also changes the concentration of DFe:

Table 1. Evidence of pronounced regional variations in the proportions of PFe (i.e., proxy for lithogenic PFe), POC (i.e., proxy for detrital PFe), and chlorophyll (i.e., proxy for algal PFe) for the four sites used in our model simulations. In all cases, the flux for each property was normalized relative to those at ALOHA (which were each arbitrarily assigned a value of 1). The normalization of lithogenic fluxes was based on regional differences in aerosol iron fluxes (i.e., reported 100-fold) range, relative to ALOHA, from Duce and Tindale (1991). The biogenic algal and detrital fluxes were scaled, relative to ALOHA, using satellite ocean color data (100-fold range from ca. 0.02 to 2.00 μg chlorophyll L^{-1}, from http://seawifs.gsfc.nasa.gov/SEAWIFS.html) and the reported downward POC fluxes (10-fold range, mmol C m^{-2} d^{-1}), respectively. Normalization to the ALOHA datasets was necessary, as the other three selected sites had insufficient data to produce the plots presented in Fig. 6b–d.

Site	Data source	Data available	Lithogenic PFe flux	Biogenic algal PFe flux	Biogenic detrital PFe flux
ALOHA (north Pacific)	Lamborg et al. (2008)	PFe, chlorophyll, and POC downward fluxes	1	1	1
NABE (northeast Atlantic)	Martin et al. (1994)	PFe and POC downward flux	0.1	100	10
BATS (northwest Atlantic)	Stanley et al. (2004); Huang and Conte (2009)	POC and PFe downward flux	10	1	1
FeCycle (southwest Pacific)	Frew et al. (2006)	PFe and POC downward flux	0.1	3	3

$$\frac{\partial C}{\partial t} = \frac{K\partial^2 C}{\partial z^2}$$

Combining mixing with input from the three iron forms, the change in DFe is

$$\frac{\partial C}{\partial t} = K\frac{\partial^2 C}{\partial z^2} - \frac{\partial F_L}{\partial z} - \frac{\partial F_D}{\partial z} - \frac{\partial F_A}{\partial z}$$

Assuming that each flux has a Martinian (Martin et al. 1987) form ($F_A = Az^{-a}$, $F_L = Bz^{-b}$, $F_D = Dz^{-d}$) and that the system is at steady state, the vertical distribution of DFe is described by

$$\frac{d^2 C}{dz^2} + \frac{aA}{K}z^{-(a+1)} + \frac{bB}{K}z^{-(b+1)} + \frac{dD}{K}z^{-(d+1)} = 0$$

The solution to this differential equation is

$$C = \frac{A}{K(1-a)}z^{1-a} + \frac{B}{K(1-b)}z^{1-b} + \frac{D}{K(1-d)}z^{1-d} + C_1 + zC_2$$

where C_1 and C_2 are constants used to fit C at the upper and lower boundaries. The constants were determined by fitting the published vertical attenuation coefficients for particle fluxes from two sediment trap array deployments at ALOHA (Lamborg et al. 2008).

We made the following assumptions to justify the selection of the proxies: lithogenic iron dominates the downward PFe flux at ALOHA and hence is approximated by the bulk flux; downward chlorophyll flux is a reliable proxy for algal PFe because most algal iron is located within the chloroplast (Strzepek and Harrison 2004); and downward POC flux provides a robust estimate of non-algal biogenic particulate flux at ALOHA (Trull et al. 2008).

The study of Lamborg et al. (2008) reported concurrent downward fluxes of PFe, POC, and chlorophyll from three depths (150, 300, and 500 m) obtained from neutrally buoyant sediment traps at ALOHA. To estimate the detrital iron flux from the POC flux of Lamborg et al. (2008) we used an Fe : C conversion factor from Frew et al. (2006) from the FeCycle experiment in HNLC waters, the only study to our knowledge to report a downward biogenic PFe flux. Frew et al. (2006) measured a downward POC flux at 120-m depth of 2.09 mmol m^{-2} d^{-1} and a biogenic PFe flux of 230 nmol m^{-2} d^{-1}, implying a detrital Fe : C ratio of (230 : 2.09) $\times$ 10^{-9} (to convert to mol Fe m^{-2} d^{-1}). The downward algal PFe flux at ALOHA was obtained by converting the downward chlorophyll flux first to carbon by assuming a C : chlorophyll (g : g) ratio of 50 (Taylor et al. 1997), and then to a PFe flux using an algal Fe : C = 5 μmol : mol for iron-replete lab cultures (Sunda and Huntsman 1995), as this region is characterized by relatively high DFe concentrations (Moore and Braucher 2008).

The relative proportions of each component of the downward PFe flux will vary among open-ocean sites, ranging from waters characterized by high dust deposition and low biological activity (Bermuda Atlantic Time Series [BATS]; Fig. 1) to intermediate dust deposition and high biological activity (North Atlantic Bloom Experiment [NABE]; Fig. 1). As a result, their relative contributions to setting the downward flux of PFe will vary (Table 1). To investigate how the relative proportions of each PFe component could differ between sites, additional model simulations were run for three other sites for which some data on PFe fluxes are available—NABE, BATS, and FeCycle (Table 1).

Because of the lack of site-specific attenuation coefficients for detrital, lithogenic, and algal PFe flux for these sites, we applied the ALOHA vertical attenuation coefficients. To compute the various PFe fluxes at each site, we scaled the PFe flux to that at ALOHA based on the proportion of the lithogenic, detrital, and algal PFe for each site (Table 1). Hence, the BATS site is characterized by high lithogenic but comparable detrital and algal iron fluxes relative to ALOHA. In contrast, the NABE site has high algal and detrital iron but low lithogenic iron fluxes compared with ALOHA, and the FeCycle site has low

lithogenic iron fluxes but elevated detrital and algal fluxes relative to ALOHA (Table 1). Although there are only limited data on vertical flux attenuance for each of these iron forms, they provide a comparison with the predicted estimates to assess the validity of this scaling approach in the model.

Results

Oceanographic setting—The PFZ study site was characterized by polar (< 4°C) HNLC waters, with DFe concentrations of < 0.2 nmol L^{-1} and chlorophyll of 0.4 μg L^{-1} within a mixed layer of 40-m depth with an underlying DCM (Bowie et al. 2009). Algal pigment data reveal that the phytoplankton community was dominated by large forms, with cells > 5 μm mainly comprised of haptophytes (50%) and with smaller fractions of diatoms and dinoflagellates (S. Wright unpubl.). Heterotrophic bacterial abundances in the surface mixed layer were 0.41 $\times$ 10^6 mL^{-1} and increased to 0.56 $\times$ 10^6 mL^{-1} in the DCM (I. Dumont unpubl.). Bacterivory by microzooplankton consumed the equivalent of 39% of daily heterotrophic bacterial production at the PFZ site (I. Pearce unpubl.).

The upper ocean at the NSAZ site was a complex transition zone between subantarctic and subtropical waters, with water temperatures of > 15°C, DFe concentrations of 0.3 nmol L^{-1}, chlorophyll concentrations of > 1 μg L^{-1}, a surface mixed layer of 25-m depth, and a DCM (Bowie et al. 2009). The phytoplankton community was dominated by large cells, and phytoplankton > 5 μm were mainly in the following chemotaxonomic algal groups: haptophyte A, dinoflagellate B, and prasinophytes (S. Wright unpubl.). Heterotrophic bacterial abundances in the mixed layer were 2.60 $\times$ 10^6 mL^{-1} and decreased with depth to 1.49 $\times$ 10^6 mL^{-1} in the DCM (I. Dumont unpubl.). Microzooplankton consumed the equivalent of 93% of heterotrophic bacterial production d^{-1} at this site (I. Pearce unpubl.).

Bacterial mobilization of algal iron—In these experiments the rates of iron uptake by phytoplankton > 5 μm in the mixed layer were 6.2 ± 0.6 nmol m^{-3} d^{-1} at the PFZ site and 8.2 ± 0.9 nmol m^{-3} d^{-1} at the NSAZ site; uptake by this size class comprised 26% and 41% of the total in the mixed layer at each site, respectively (Bowie et al. 2009). By the end of the 72-h incubation, of the iron initially taken up, ~ 40% had been remineralized at the PFZ site and ~ 60% at the NSAZ site (Fig. 3a,c). At both sites, the relatively rapid transfer of ^{55}Fe label from the > 5-μm fraction into the bacterial fraction and the dissolved phase (i.e., < 0.2-μm fraction; Fig. 2) suggests rapid colonization of the phytoplankton cells by heterotrophic bacteria. The mobilized iron was probably derived from both within and without the algal cells; however, it was not possible to discriminate between intra- and extracellularly bound iron (*see* Fig. 2 caption).

For experiments conducted at both sites, there was little evidence of the transfer of label into the intermediate size fraction (Fig. 3); this is interpreted as evidence of little subsequent bacterivory of labeled cells in the bacterial fraction (Fig. 2). The retention of radioisotope activity in the algal fraction is more difficult to interpret. There are at least three possible pathways: retention of ^{55}Fe within phytoplankton cells; bacterial colonization of the algal cells and transfer of label to attached bacteria; and/or herbivory by grazers > 5 μm resident within the initial incubation seed stock. Without the availability of a more powerful diagnostic on the vessel, such as autoradiography or epifluorescence microscopy, it was not possible to resolve this issue.

In water taken from the DCM at both sites, rates of iron uptake by phytoplankton > 5 μm were 3.1 ± 0.5 nmol m^{-3} d^{-1} at the PFZ site and 4.7 ± 0.3 nmol m^{-3} d^{-1} at the NSAZ site, comprising 35% and 85% of algal community iron uptake at the DCM over a 24-h period at each site, respectively (Bowie et al. 2009). At the PFZ site, the size partitioning of the radiolabel initially in the algal fraction increased in the bacterial fraction from the initial 0% to 12% after 24 h and increased to 24% by 72 h (Fig. 3b). There was evidence of a small increase (< 5%) in the ^{55}Fe label within the intermediate and dissolved fractions at this site. In general, the recovery of the label (relative to that in the time zero replicates) ranged between 85% and 114% and was comparable to that reported for other such ^{55}Fe manipulative experiments using marine biota (Strzepek et al. 2005).

In contrast, there was marked mobilization at the DCM of the NSAZ site of much of the iron initially taken up by the algal fraction. Over 20% was located within the bacterial fraction after 24 h, rising to 41% after 72 h (Fig. 3d). At the final time point of 72 h, 22% of the ^{55}Fe was within the intermediate fraction, suggesting that bacterivores may have been present at higher abundances within the initial seed stock on the 5-μm filters. These findings are consistent with the higher rates of bacterivory measured at the NSAZ site relative to the PFZ site (I. Pearce unpubl.). The highest mobilization of labeled iron within the algal size class was evident at the DCM at the NSAZ site.

DFe and iron-binding ligand release experiments—The experiments at both the PFZ and NSAZ sites produced similar trends from each of the treatments for mobilization of DFe and the concurrent release of iron-binding ligands. There was no significant change in concentrations of either DFe or iron-binding ligands in the seawater-only controls (Fig. 4; Tables 2, 3). This was also the result at each site for the abiotic treatments with heat-sterilized particles, suggesting that this treatment did not result in significant lysis of cells and, hence, release of iron and/or ligands (Fig. 4). In contrast, there were significant increases in the concentrations of both DFe and weaker ligands L2 (i.e., no L1 was detected; *see* Tables 2, 3) over the 12-d incubation at the PFZ site, with the release of DFe being slightly faster in the 8°C incubation than in the 4°C incubation (Fig. 4a,b). The quasi-linear temporal trend in concentration at this site suggests a constant release rate. In both these temperature treatments, the increase in L2

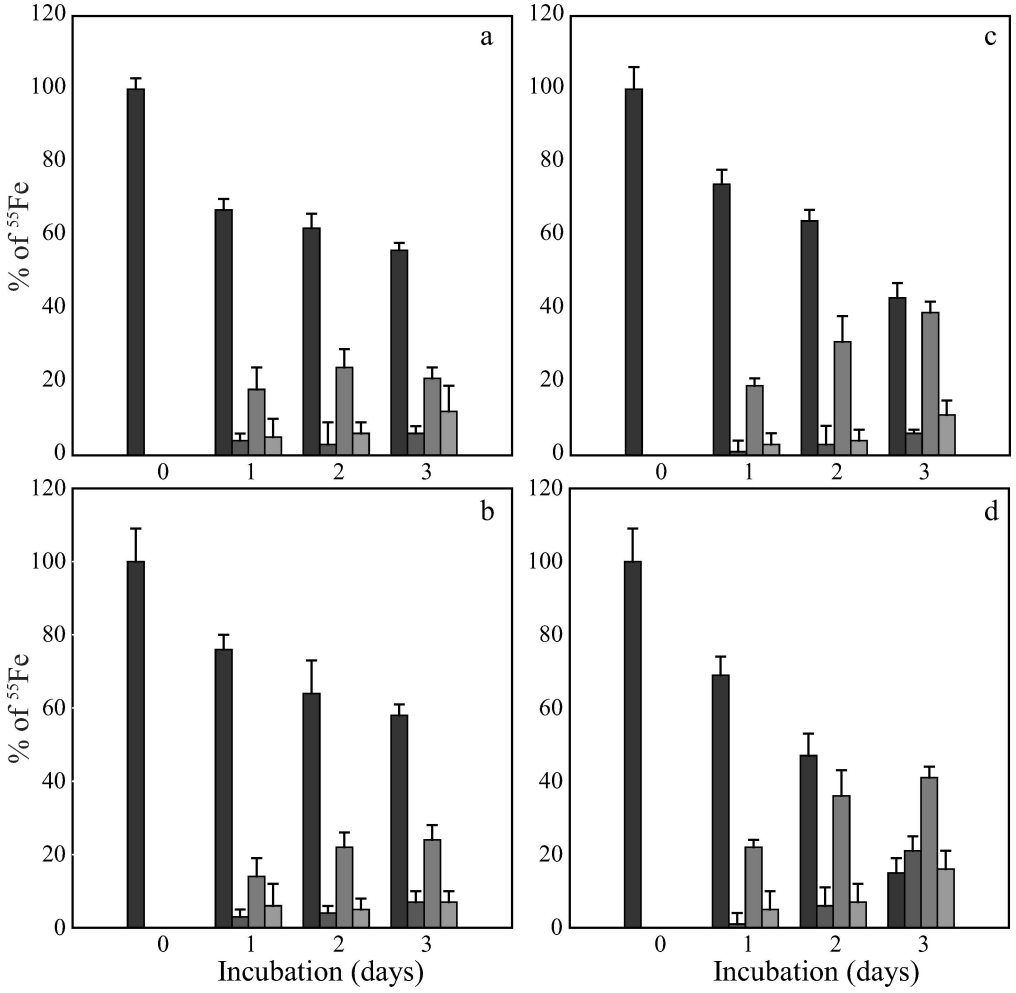

Fig. 3. Time series of the partitioning of radiolabeled iron between different size fractions at the (a, b) PFZ and (c, d) NSAZ sites (from left to right for each bar cluster: algal; intermediate; bacterial; dissolved fractions at 0, 24, 48, and 72 h during incubations in darkness and at ambient temperatures). (a, b) display the time series for surface mixed-layer (SML) and deep chlorophyll maximum (DCM) incubations, respectively. (c, d) display those for the SML and DCM strata, respectively. There was no evidence of significant abiotic mobilization of the labeled Fe (i.e., $< 3\%$ of the radioactive activity measured in the < 1.0-μm-filtered seawater treatment) in a further treatment using 0.2-μm-filtered seawater as the incubation medium (data not shown). The error bars represent the standard error of the mean of three pseudo-replicates.

concentrations was greater, and occurred more rapidly, than that recorded for DFe.

At the NSAZ site, there was evidence of similar temporal trends to the PFZ site for L1 (none detected; Table 3). Increases in both L2 and DFe concentrations were apparent during the 5-d incubation in the treatments with biogenic particulates, with that for L2 greater than that for DFe (Fig. 4c,d). Although the incubations were run for different durations (12 d at PFZ vs. 5 d at the NSAZ site) there were similar increases in both the L2 and DFe concentrations, and thus faster release rates at the NSAZ site. This trend may again reflect the higher incubation temperatures (i.e., enhanced heterotrophic bacterial enzymatic activity; Bidle et al. 2002), or higher bacterial abundances at depth at the NSAZ site (I. Dumont unpubl.).

Model simulations of PFe remineralization—The use of proxies for the various components of PFe downward flux in this simple model enables the incorporation of both the attenuation of each flux and its relative contribution to total PFe flux (Fig. 5). The downward flux profiles illustrate the different rates of flux attenuation for the various components of PFe at ALOHA, with the chlorophyll (i.e., algal iron) flux having the most rapid vertical attenuation, followed by the POC (i.e., detrital iron) flux and then the lithogenic (i.e., bulk iron) flux (Fig. 5a–c). The resulting contribution to the PFe downward flux by each component is presented in Fig. 5d. At ALOHA, lithogenic iron dominates the export signal, with both detrital and algal iron being relatively small fractions.

This trend was not always observed at the other sites, with detrital iron making the largest contribution to the downward PFe flux, down to 150-m depth, at the HNLC FeCycle site in the subantarctic Pacific, and detrital iron dominating the PFe flux at the NABE site in spring (Fig. 6b,c). As expected, lithogenic iron dominated the PFe

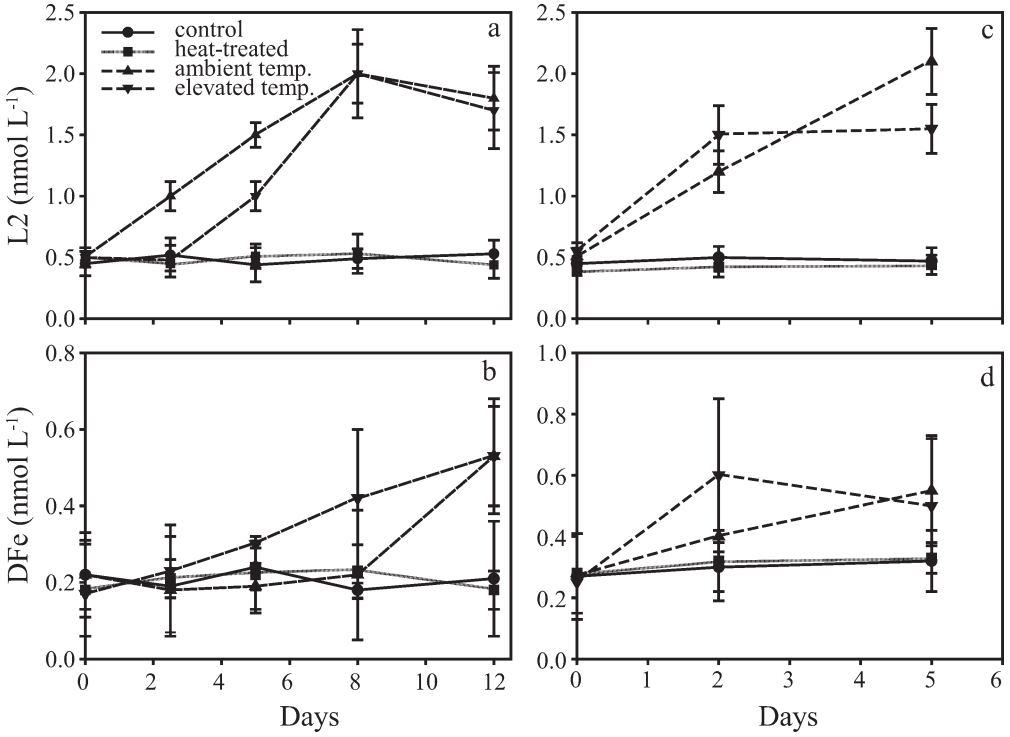

Fig. 4. Release of iron-binding ligands and DFe from PFe at the (a, b) PFZ and (c, d) NSAZ sites. The four treatments are a control (no particles), a heat-treated suspension of particles > 53 μm, and a suspension of particles > 53 μm incubated under conditions of darkness at both ambient (4°C, PFZ; 8°C, NSAZ) and elevated temperatures (8°C, PFZ; 15°C, NSAZ). (a, c) present the release of L2, and (b, d) present the DFe release. The error bars for log *K*'s and L's represent two times the standard deviation of the nonlinear fit of the Gerringa plot. The error bars for DFe represent two times the standard deviation of three replicate determinations. Note: no data were available for DFe and L2 for time zero for the elevated temperature treatment in (c, d) so we have used the time zero data for the ambient temperature treatment for both sites and assumed that they are comparable. The plotted data and ancillary information, for example on the conditional stability constants, are presented in Tables 2, 3.

flux at the BATS site in the subtropical northwest Atlantic (Fig. 6d), which receives a high aerosol dust input (Duce and Tindale 1991). Hence, for this wide range of sites, different components of the PFe flux will dominate, with implications for the biogeochemistry of iron.

The dissolution of iron from sinking PFe is set by both the magnitude of PFe flux (Fig. 6) and the vertical attenuation rates of this flux for each component of the PFe, with algal > detrital > lithogenic (Figs. 5, 6). Sites dominated by the lithogenic flux will have a smaller proportion of dissolution per unit PFe flux as particles settle to depth than sites dominated by detrital iron. The PFe component that dominates iron dissolution from settling particles varies between sites, being the lithogenic fraction at BATS and ALOHA, and the detrital fraction at the NABE and FeCycle sites (Fig. 7).

Rates of DFe iron supply from remineralization ranged from 100 pmol L^{-1} d^{-1} between 100 and 200 m at BATS to 6 pmol L^{-1} d^{-1} at the FeCycle site over this depth range (Fig. 7). Significantly, the release of DFe was mainly (98%) from the lithogenic PFe component at BATS, where the magnitude of this PFe flux compensates for its relatively low dissolution rate. In contrast, at the FeCycle site detrital PFe comprised 86% of the release of DFe, and although the bulk PFe flux was relatively small compared with that at BATS, the detrital component of PFe has a higher dissolution rate than lithogenic PFe. The algal PFe flux made an insignificant contribution to dissolution at all sites, even though it has the highest relative dissolution rate. Such a rapid attenuation in algal PFe could make the dissolution of this component dominant in the upper 100 m.

Discussion

Heterotrophic bacterial mobilization of algal iron—There was indirect evidence of relatively rapid bacterial colonization of the mixed phytoplankton assemblage and mobilization of algal iron into the bacterial fraction by the first sampling point after 24 h at both these Southern Ocean sites. It is possible to compare our results with only one other study on bacterial colonization of oceanic particles. Bidle and Azam (1999) found a similar pattern of rapid mobilization of Si, via dissolution of diatoms and their constituents for laboratory cultures, with biogenic silica turnover rates of 2–18% d^{-1} on days 0–2, and with rates varying with the diatom species studied. They reported that biogenic silica rates slowed to 0.8–3.2% d^{-1} after day 2. Bidle and Azam also observed the fast and slow phases in the disappearance of diatom cells and of their chlorophyll, with 60% lost within 2 d, but the remaining fraction taking a further 5–20 d to disappear. This broad range for the

Table 2. Conditional stability constants for iron-binding ligands, and ancillary information on iron chemistry, observed during the ligand production experiments at the PFZ site. Strong binding ligands L1, defined as those having a log $K_{FeL1,Fe3+} > 22$, were absent in all samples. FeL2 is the percentage of DFe present as complex with L2, Fe′ is the concentration of free dissolved iron. The error for log *K*'s and L's is two times the standard deviation of the nonlinear fit of the Gerringa plot. The error for DFe is two times the standard deviation of three replicate determinations.

Days	DFe (nmol L^{-1})	L2 (nmol L^{-1})	Log $K_{FeL2,Fe3+}$	FeL2 (%)	Fe′ (pmol L^{-1})
Control (4°C)					
0	0.23±0.09	0.57±0.10	20.88±0.28	96.08	9.18
2.5	0.23±0.13	0.57±0.08	21.60±0.28	99.26	1.70
5	0.24±0.06	0.57±0.14	21.30±0.30	98.47	3.70
8	0.30±0.02	0.50±0.08	21.20±0.32	96.86	9.39
12	0.26±0.15	0.62±0.11	20.92±0.30	96.68	8.57
Microwaved samples with particles (4°C)					
0	0.23±0.09	0.57±0.10	20.88±0.28	96.08	9.18
2.5	0.23±0.13	0.57±0.08	21.60±0.28	99.26	1.70
5	0.24±0.06	0.57±0.14	21.30±0.30	98.47	3.70
8	0.30±0.02	0.50±0.08	21.20±0.32	96.86	9.39
12	0.26±0.15	0.62±0.11	20.92±0.30	96.68	8.57
Samples with particles (4°C)					
0	0.23±0.11	0.70±0.08	21.09±0.26	98.27	3.98
2.5	0.19±0.02	0.70±0.12	21.76±0.20	99.66	0.63
5	0.32±0.06	1.07±0.10	21.86±0.22	99.82	0.59
8	0.61±0.17	1.97±0.36	20.95±0.26	99.18	5.01
12	0.54±0.13	1.79±0.26	21.09±0.28	99.35	3.47
Samples with particles (8°C)					
0	—	—	—	—	—
2.5	0.24±0.03	1.19±0.16	21.01±0.23	98.96	2.44
5	0.35±0.01	1.49±0.12	21.09±0.14	99.29	2.52
8	0.47±0.18	1.99±0.24	21.00±0.18	99.34	3.07
12	0.55±0.15	1.74±0.31	20.83±0.28	98.74	6.90

remaining fraction to dissolve was also due to species dependence.

We estimated an iron mobilization rate from the transfer of label initially in the algal fraction to the bacterial fraction. The rates for our mixed algal community ranged from $< 5\%$ to 17% d^{-1} over 72 h, but we did not observe the two distinct phases of remineralization by bacteria reported by Bidle and Azam (1999). The mobilization rate was greatest at the NSAZ site, which was characterized by both warmer upper ocean temperatures and higher abundances of heterotrophic bacteria than at the PFZ site. Bidle et al. (2002) have reported that increased tempera-

Table 3. Conditional stability constants for iron-binding ligands and ancillary information on iron chemistry observed during the ligand production experiments at the NSAZ site. Strong binding ligands were absent from all samples.

Days	DFe (nmol L^{-1})	L2 (nmol L^{-1})	Log $K_{FeL2,Fe3+}$	FeL2 (%)	Fe′ (pmol L^{-1})
Control (8°C)					
0	0.30±0.14	0.42±0.06	21.83±0.48	98.77	3.70
2	0.31±0.08	0.70±0.09	21.52±0.27	99.23	2.35
5	0.29±0.11	0.81±0.11	21.47±0.29	99.34	1.94
Microwaved samples with particles (8°C)					
0	0.21±0.09	0.29±0.04	21.07±0.28	89.01	23.13
2	0.29±0.10	0.37±0.08	21.65±0.38	97.20	8.12
5	0.30±0.05	0.78±0.08	21.34±0.22	99.05	2.83
Samples with particles (8°C)					
0	0.26±0.13	0.49±0.07	21.52±0.35	98.67	3.45
2	0.41±0.21	1.25±0.17	20.98±0.19	98.74	5.22
5	0.59±0.18	1.97±0.27	20.97±0.21	99.22	4.54
Samples with particles (15°C)					
0	—	—	—	—	—
2	0.62±0.25	1.50±0.24	20.99±0.22	98.83	7.21
5	0.54±0.22	1.56±0.20	20.88±0.20	98.71	6.91

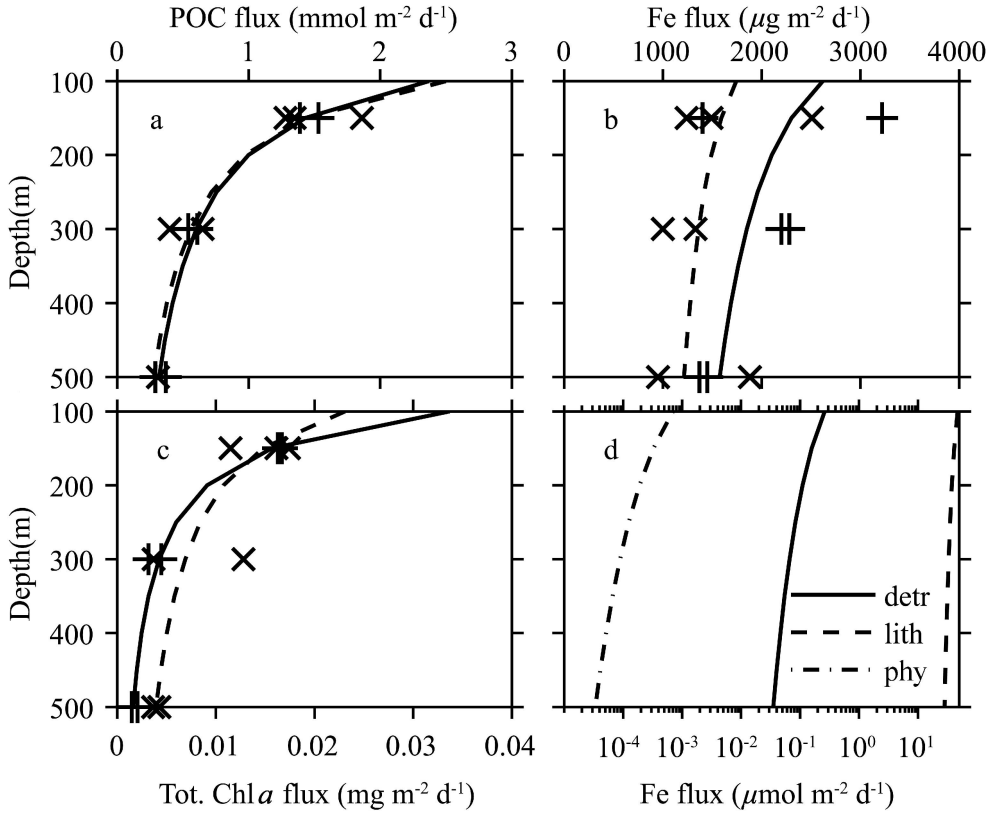

Fig. 5. Downward particulate fluxes associated with different iron fractions at ALOHA. (a) POC flux (proxy for detrital iron); (b) iron flux (proxy for lithogenic iron flux); (c) chlorophyll *a* flux (proxy for algal iron) redrawn from Lamborg et al. (2008). The attenuation of each flux was then calculated from the Martin et al. (1987) equation and fitted for the first neutrally buoyant sediment trap (NBST) deployment reported in Lamborg et al. (d) These flux curves were then converted to common Fe equivalents (*see* main text for details; detr denotes biogenic detrital iron; lith denotes lithogenic iron; phy denotes phytoplankton iron). +, x denote observations from first and second NBST deployments; (a–c) solid and dashed lines represent the lines fitted for the first and second NBST deployments, respectively.

tures elevated the bacterial remineralization rates of diatoms.

At both of the depths sampled at the PFZ and NSAZ sites, there was little evidence of significant accumulation of ^{55}Fe label in the dissolved fraction. This observation is consistent with the absence of grazers in the water filtered to remove particles < 1 μm in the experiments. In contrast, Strzepek et al. (2005) reported a pronounced increase in radiolabeled iron in the < 0.2-μm fraction for bacterivory experiments in HNLC waters. They suggested that such iron accumulation indicates that this lysed iron is not bioavailable, possibly as a result of the concurrent release of colloidal and/or dissolved organic ligands (Twiss and Campbell 1995). Although the design of our study did not permit investigation of such concurrent release of iron-binding ligands during this mobilization of iron, other grazing studies have reported the release of ligands (Sarthou et al. 2008). Sarthou et al. (2008) conducted iron remineralization experiments near Kerguelen (Fig. 1) during the Kerguelen Ocean and Plateau Compared Study (KEOPS). They observed that $< 1\%$ of the regenerated iron (resulting from copepod grazing) was complexed with hydrophobic organic ligands (using C18 columns) and suggested that the mobilized iron was released either as ligands (soluble organic) or as inorganic iron species.

Breaking the microbial loop influence on the ferrous wheel?—To explore the role of heterotrophic bacteria in remineralizing algal iron, our experimental design used $<$ 1-μm filtrate for incubations, removing larger components of the microbial loop, such as microzooplankton, from the 72-h incubation with heterotrophic bacteria. The experiments were also incubated in darkness to prevent further uptake and transfer of label by phytoplankton. This step may have removed the potential influence of photochemistry on iron bioavailability during these experiments (Barbeau 2006) and/or on the dissolution of algal detritus (Mayer et al. 2009). These experimental artifacts mean that we may have overestimated iron remineralization by bacterial activity because of the absence of bacterivores. However, we also cannot rule out that the degree of iron bioavailability of the mobilized ^{55}Fe may have been reduced, relative to that in situ, during our incubations in darkness.

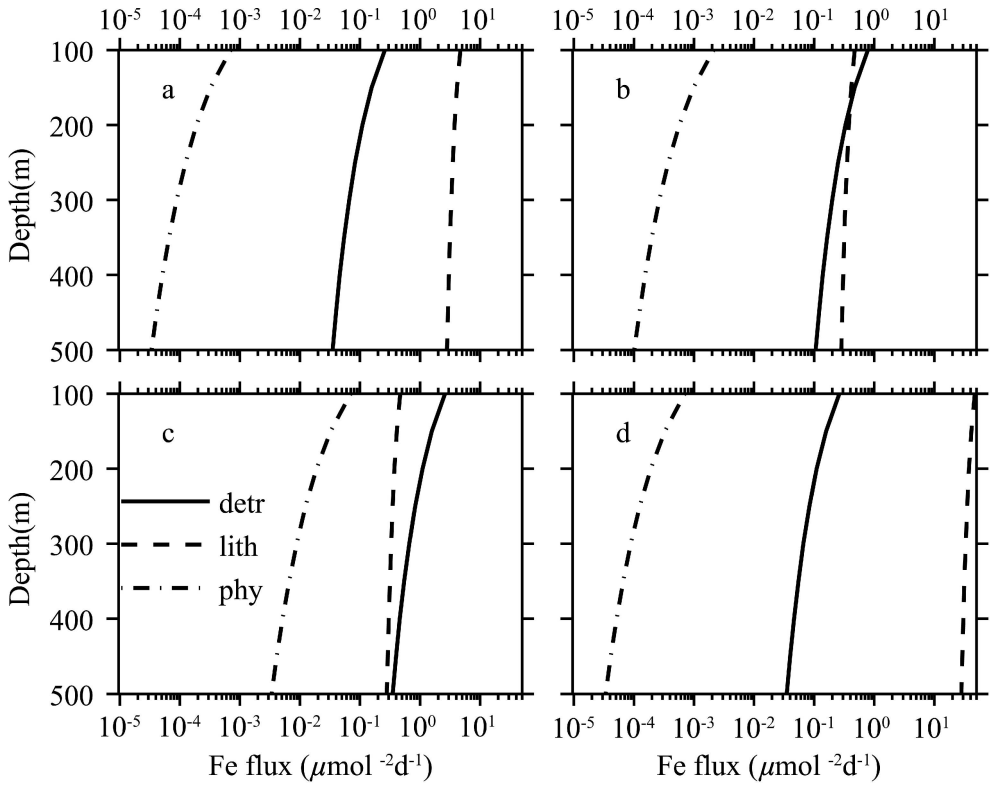

Fig. 6. Particulate iron fluxes estimated for the algal, detrital, and lithogenic components at the four selected locations. (a) ALOHA (subtropical North Pacific gyre; note that this panel is identical to that in Fig. 4d); (b) FeCycle (subantarctic Pacific Ocean); (c) NABE (northeast Atlantic Ocean); (d) tropical Atlantic Ocean. Solid line denotes detrital PFe; dashed line denotes lithogenic PFe; and dash–dot line denotes algal PFe. Fluxes for ALOHA were calculated from observations from Lamborg et al. (2008), as in Fig. 5. Fluxes for other locations were estimated from the ALOHA curves assuming multiplicative factors given in Table 1. detr denotes biogenic detrital iron; lith, lithogenic iron; phy, phytoplankton iron.

We can compare our observed iron mobilization rates with those from studies in which micrograzers were not removed (Strzepek et al. 2005; Sarthou et al. 2008). Both of these experiments were conducted in Southern Ocean waters, and hence are comparable systems to those investigated in the present study. Strzepek et al. measured both bacterivory and herbivory during the FeCycle study and reported rapid turnover of both bacterial and algal iron, with the ferrous wheel spinning rapidly (hours to days) in these HNLC waters. Sarthou et al. (2008) reported daily iron regeneration rates by both microzooplankton and, to a lesser extent, mesozooplankton that were comparable to the daily iron requirements of the resident phytoplankton in both HNLC and high-iron waters near Kerguelen. In contrast, we observed significant mobilization of iron by heterotrophic bacteria but at relatively slower rates (2–3-fold slower) than in these other Southern Ocean field studies by Strzepek et al. (2005) and Sarthou et al. (2008). Our only evidence for a comparable rate of iron mobilization, relative to the requirements of primary producers, was in a time-series sample at the DCM at NSAZ, where there was a significant transfer of label to the intermediate fraction after 72 h. This result is most likely due to an increase in the abundance of heterotrophic nanoflagellates initially present in small abundances of the algal fraction during the 3-d incubation. The rates of bacterivory by microzooplankton at this site were highest for all of the SAZ-SENSE study sites (I. Pearce unpubl.).

The comparison of our rates of bacterial iron mobilization with those in other grazing studies points to the key role of grazers in mobilizing iron in the surface ocean, and indicates that by breaking the microbial loop in our experiments, we slowed the spinning of the ferrous wheel. This in turn may provide insights into the observed differences between rates of PFe remineralization in the surface mixed layer vs. the subsurface ocean.

Release of L2 and DFe during particle remineralization—There have been previous reports of the release or production of weak iron-binding ligands, either as cell debris, such as porphyrin rings (Hutchins et al. 1999), or as humic substances in coastal waters (Laglera and van den Berg 2009). However, the present study is the first to our knowledge to present evidence of the release of weak iron-binding ligands during the bacterial remineralization of particles. Recent iron biogeochemical modeling studies have attempted to incorporate some representation of ligand dynamics (Moore and Braucher 2008). In particular,

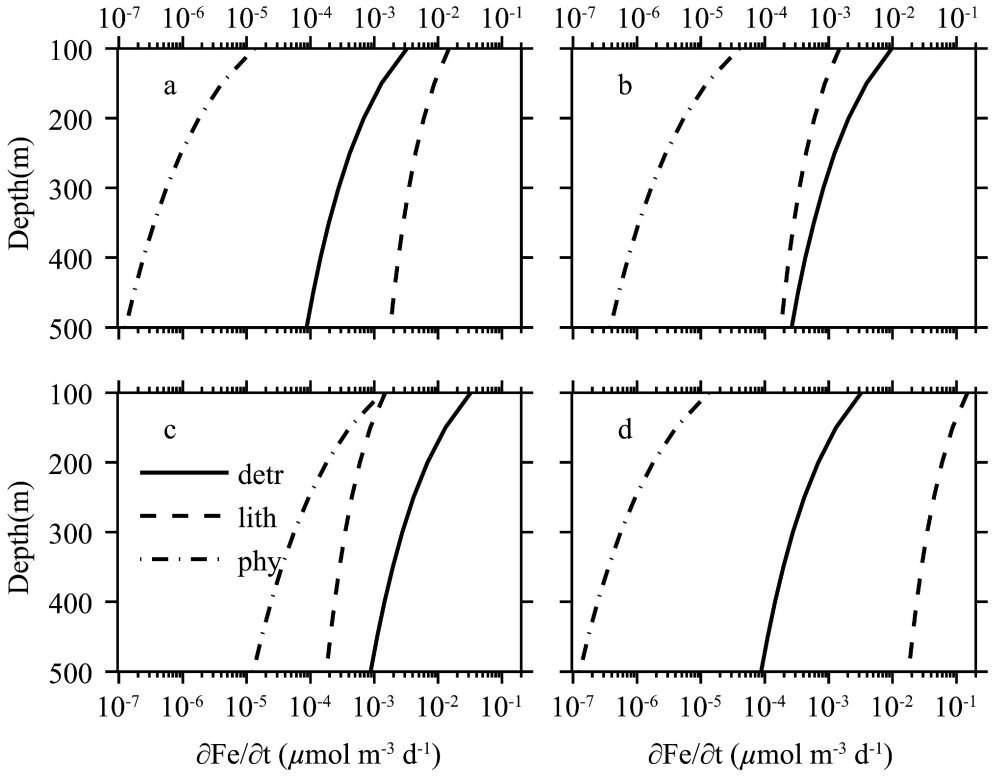

Fig. 7. Estimated rate of DFe iron supply from particle dissolution for the different particle fractions at four locations. (a) ALOHA station; (b) FeCycle; (c) NABE; (d) tropical Atlantic Ocean. Solid line, from detrital particles; dashed line, from lithogenic particles; dash–dot line, from phytoplankton particles. Dissolution rate was calculated as $b \times$ flux, where the flux $= B z^{-b}$. detr denotes biogenic detrital iron; lith, lithogenic iron; phy, phytoplankton iron.

Parekh et al. (2004) compared three different model simulations that featured either scavenging, scavenging and subsequent desorption, or the inclusion of iron-binding ligands as a threshold that had to be exceeded to permit iron scavenging. Our findings suggest that the last of these ligand dynamics models is most appropriate but that issues remain regarding the use of a ligand threshold (Moore and Braucher 2008).

The particles used in the incubations at both sites were $>$ 53 μm and hence should be mainly sinking particles (based on Stokes' Law). Using data on PFe concentrations at each of these sites from Bowie et al. (2009), in conjunction with estimates of the relative contribution of $>$ 53-μm PFe to the total PFe inventory (Frew et al. 2006) for a similar subantarctic site, we estimated the release rates of both DFe and weak iron-binding ligands (Table 4).

In each incubation, the release rates for DFe and weak iron-binding ligands were calculated from the amount of PFe in the particles ($>$ 53 μm) added to each experimental treatment (Table 4). In the absence of data on the relative proportion of biogenic vs. lithogenic PFe fluxes or on the ligand inventory of the particles, we had to assume that all of the PFe could potentially be remineralized by the heterotrophic bacteria, and that the specific particulate source (i.e., PFe vs. POC vs. particulate organic matter) for iron-binding ligands was unknown (*see* Table 4 legend). The release rates for DFe of 1.4% PFe inventory d^{-1} (PFZ) and 1.6% PFe inventory d^{-1} (NSAZ) were less than those for the iron-binding ligands (7.0% [at PFZ]; 8.6% [at NSAZ]). This trend is expected, because ligand concentrations were always observed to be in excess of DFe concentrations in vertical profiles to 1000-m depth at both sites during the SAZ-SENSE study (Ibisanmi et al. in press).

These DFe release rates correspond to 0.2 and 0.6 pmol DFe L^{-1} d^{-1} at the PFZ and NSAZ sites, respectively (*see* Table 4). To compare these rates with in situ PFe remineralization rates from upper-ocean free-drifting sediment traps requires data on downward PFe fluxes from 2 depths; Bowie et al. (2009) measured the PFe flux only at 150-m depth, so we have taken data from the FeCycle study (Fig. 1; Frew et al. 2006) to estimate this DFe release rate. Frew et al. (2006) reported a decrease in PFe flux between 80-m and 120-m depth of 198 nmol m^{-2} d^{-1} (from 548 to 350 nmol m^{-2} d^{-1}), corresponding to a DFe release rate of 5.0 nmol m^{-3} or 5 pmol L^{-1}. Our estimated rates of DFe release are around an order of magnitude lower than estimated from the sediment trap measurements. Moreover, our relatively low DFe release rates ($<$ 2% PFe d^{-1}) are in marked contrast to the rapid mobilization of iron within the ferrous wheel in the surface mixed layer (Fig. 3).

Residence time of DFe in the subsurface ocean—A comparison of our rates of DFe release at each site with the

Table 4. Calculations to derive estimates of the daily release of DFe and weak iron-binding ligands from the incubated > 53-μm PFe samples. Rates for DFe release were expressed both as a percentage of the PFe in the incubation vessel and as DFe released per liter per day. Rates of ligand "release" were only expressed as the former. PFe concentrations were obtained from Bowie et al. (2009) at our sample depths. The proportion of particles > 53 μm at our sites was assumed to be comparable to that at an HNLC site in the northeast subarctic Pacific. Boyd et al. (1999) reported that particles > 53 μm consistently made up 20% of the total particle population from 0 to 1000-m depth. The DFe release rate assumes all PFe was available to be remineralized, i.e., DFe released : PFe available. The DFe and L2 release rates in parentheses have been corrected for the particle concentration factor (i.e., PFe in the incubation vessel : [PFe] at sampling depth), and were used to estimate the residence time of DFe and L2 in the subsurface ocean. As there are many potential sources of weak ligands in the debris associated with sinking particles as they are broken down (Hutchins et al. 1999), we cannot estimate an L2 release as a percentage.

Site	[PFe] at sampling depth (nmol L^{-1})	Volume filtered (liters) : resuspension volume (liters)	PFe in incubation vessel (nmol L^{-1})	Incubation period (d)	Increase in DFe (nmol L^{-1})	Increase in L2 (nmol L^{-1})	DFe release rate (% d^{-1})	L2 release rate (pmol L^{-1} d^{-1})	DFe release (pmol L^{-1} d^{-1})
PFZ	0.10	803 : 9 = 89.2	1.8	12	0.31	1.5	1.4	1303(7.2)	25.8(1.4)
NSAZ	0.20	835 : 9 = 92.8	3.7	5	0.33	1.6	1.8	300(16.2)	66.0(3.6)

respective DFe inventory enabled the estimation of the residence time of DFe in the 100–130-m depth range, i.e., the waters immediately above and below where we sampled the sinking particles. Bowie et al. (2009) present vertical profiles of DFe for the PFZ and NSAZ sites. We used these data to compute the water column inventory for the 100–130-m depth range. At the PFZ site, the inventory was 6 μmol Fe m^{-2}, compared with a column-integrated DFe release from PFe of 42 nmol Fe m^{-2} d^{-1} (*see* Table 4). This gives a residence time of 0.4 yr at the PFZ site, assuming that the system is in steady state, and that sinking particles supply all of the DFe released. At the NSAZ the residence time is 0.2 yr, based on a DFe inventory of 9 μmol Fe m^{-2} and a column-integrated DFe release rate of 108 nmol Fe m^{-2} d^{-1}. These residence time estimates for HNLC waters compare with 1.4 yr for the upper ocean (i.e., to 103-m depth) in a low-iron region from model simulations (*see* table 4 of Moore and Braucher 2008). It is likely that our release rates diverge from the modeled estimates because they cannot take into account several factors: lateral or vertical advection of DFe (Boyle 1997); bacterial uptake of the mobilized iron following its release; any deleterious pressure effects on the particles and bacteria collected from 120-m depth but incubated at atmospheric pressure (Boyd et al. 1999); and the assumption that all of the DFe inventory is from recently released material. Based on the column-integrated ligand release rates (Table 4) and ligand inventory (Ibisanmi et al. in press), the residence time of the weak iron-binding ligands is of the same order as for DFe, i.e., months.

The role and source of weak iron-binding ligands—Weak iron-binding ligands are the dominant ligand form in the subsurface ocean, whereas strong iron-binding ligands dominate in the upper ocean (Rue and Bruland 1995; Hunter and Boyd 2007). Our experiments present the first evidence of the source of these weak ligands—release during particle remineralization by bacteria. Such ligand production at depth plays a key role in preventing the scavenging onto settling particles of DFe released during remineralization by microbial populations. This permits iron to be remineralized and subsequently resupplied to the surface ocean either by upwelling or by deepening of the surface mixed layer over winter. When resupplied to the upper ocean, the iron can be stripped off the weak ligands by stronger ligands such as siderophores via competitive ligand exchange in the mixed layer (Mawji et al. 2008). Our iron-binding ligand release experiments cannot provide any insights into whether the ligands released were soluble or colloidal. Subsequent experiments should try to better characterize the size class of the released ligands, as this may have major implications for the interplay between scavenging of DFe (bound to colloidal ligands) and the maintenance of DFe in the water column (Moore and Braucher 2008).

The likely source of these ligands (and also the DFe) is from the detrital PFe, which contributes most to PFe export flux in Southern Ocean waters (Fig. 6b; Frew et al. 2006; Sarthou et al. 2008). The study of Frew et al. (2006) is one of the few to provide estimates of how both biogenic

Table 5. A comparison of the attenuation coefficients for algal (i.e., using downward chlorophyll flux), detrital (i.e., POC flux), and lithogenic (i.e., bulk PFe flux) PFe from ALOHA (Lamborg et al. 2008) that were applied to the four sites used in model simulations with those available from sediment trap studies at these sites. The attenuation coefficients are expressed as b values following the convention in the Martin et al. (1987) study, in which they used a power law formulation $F/F_{100} = (z/100)^{-b}$ (F_{100} is flux at a reference depth of 100 m; F is the flux of another sediment trap at a depth z) to describe decreases in the downward particle flux with depth. Larger b values denote more rapid attenuation of the particle flux and vice versa. na denotes not available because of insufficient sampling—such as for the Martin et al. (1994) study at the NABE site, in which the PFe flux was measured at only one depth (150 m).

Site	Algal PFe	Detrital PFe	Lithogenic PFe	Bulk PFe	References
ALOHA	1.70	1.30	0.32	0.32	Lamborg et al. (2008)
BATS	na	0.32		Increase with depth*	Stanley et al. (2004); Huang and Conte (2009)
FeCycle	na	1.70	0.25	0.64	Frew et al. (2006)
NABE	na	1.10	na		Martin et al. (1994)

* This flux increases with depth, indicative of lateral iron supply; therefore, a conventional b value cannot be fitted.

and lithogenic PFe fluxes decrease with depth. Frew et al. reveal that whereas there was a 50% decrease in the biogenic PFe flux in the 40 m between traps at 80 m and 120 m at the FeCycle site (Fig. 1), there was only an 11% decrease in the lithogenic flux over this depth range. These differences support our contention that biogenic rather than lithogenic PFe is the source of DFe and weak iron-binding ligands at both of our study sites. Differences between biogenic and lithogenic particles should affect the relative proportions of DFe and ligands released during PFe remineralization in high-iron and low-iron regions of the ocean. For example, although lithogenic PFe is predicted to contribute 98% of DFe release at the BATS site (Fig. 7), if there is no concurrent release of L2 ligands during remineralization, subsequent scavenging onto settling lithogenic particles is the probable fate of this released DFe. This supports the conclusion of Moore and Braucher (2008) that scavenging is likely to be a more important process in high-iron regions after they ran a suite of modeling simulations.

Our findings about ligand and DFe release from sinking particles disagree in part with the explanation of Frew et al. (2006) that fourfold increases in the Fe : C ratio of sinking particles between the mixed layer and 120-m depth were due solely to the different fates of POC (bacterial solubilization to dissolved organic carbon) and PFe (desorption followed by sorption onto the particle). Frew et al.'s interpretation does agree with a longer remineralization length scale for iron relative to macronutrients and a resulting deeper ferricline than nutricline (Boyd et al. 2005). We suggest that the lack of vertical decrease of the lithogenic PFe flux in HNLC waters (*see* Table 5) could mask important changes in the PFe downward flux (Fig. 6).

Model simulations of PFe remineralization—Our simple model clearly demonstrates how the interplay of different vertical attenuation coefficients that characterize algal, detrital, and lithogenic PFe, in combination with their different contributions to downward PFe flux, influences the dissolution of DFe at different sites in the subsurface ocean. Although there are many gaps for b (index of vertical attenuance; Martin et al. 1987) in published sediment trap datasets, there are some encouraging trends with comparable b values between those used in the model (based on the ALOHA datasets) and those at the FeCycle site for lithogenic PFe fluxes and at the NABE and FeCycle sites for detrital PFe fluxes (Table 5). In contrast, the sole reported attenuation coefficient from BATS is much smaller for detrital Fe than that used in the model. More datasets are required to better evaluate the validity of applying the ALOHA b values to other open-ocean sites.

Johnson et al. (1997) used a similar particle attenuation approach for modeling. However, it is difficult to compare and contrast the model results, as Johnson et al. focused only on bulk PFe flux and examined global patterns in deep-ocean DFe concentrations and regional variations in DFe vertical profiles. In contrast, our model simulations explore the implications of different components of the PFe export flux for remineralization in the upper 500 m of the open ocean.

Our field results suggest that models that have attempted to incorporate ligand dynamics need to be refined by including the concurrent release of weak iron-binding ligands in subsurface waters. Parekh et al. (2004) used a range of dissolution schemes, including the incorporation of different adsorption and desorption processes such as scavenging and/or ligands, but did not subdivide the PFe flux into components with different lability, nor did they consider the weaker ligands. Our model needs to be expanded to include more realistic ocean physics, including vertical advection of receiving water (Boyle 1997). Other aspects of the flux that need to be explored include explicit consideration of processes such as coagulation or adsorption.

A conceptual model of iron remineralization—The FeCycle study (Fig. 1) showed the importance of both PFe inventory and fluxes in the upper ocean for the biogeochemical iron cycle (Boyd et al. 2005; Frew et al. 2006). There was evidence of a relatively long residence time for aerosol iron, of transformation of lithogenic particulates to biogenic particulates in the surface mixed layer, and of little vertical attenuance of PFe fluxes despite fast pelagic iron recycling within a rapidly spinning ferrous wheel (Strzepek et al. 2005).

We can reappraise the findings from FeCycle and attempt to develop a new conceptual model in which we incorporate the various roles of algal, detrital, and lithogenic PFe on iron biogeochemistry (Fig. 8a). Hetero-

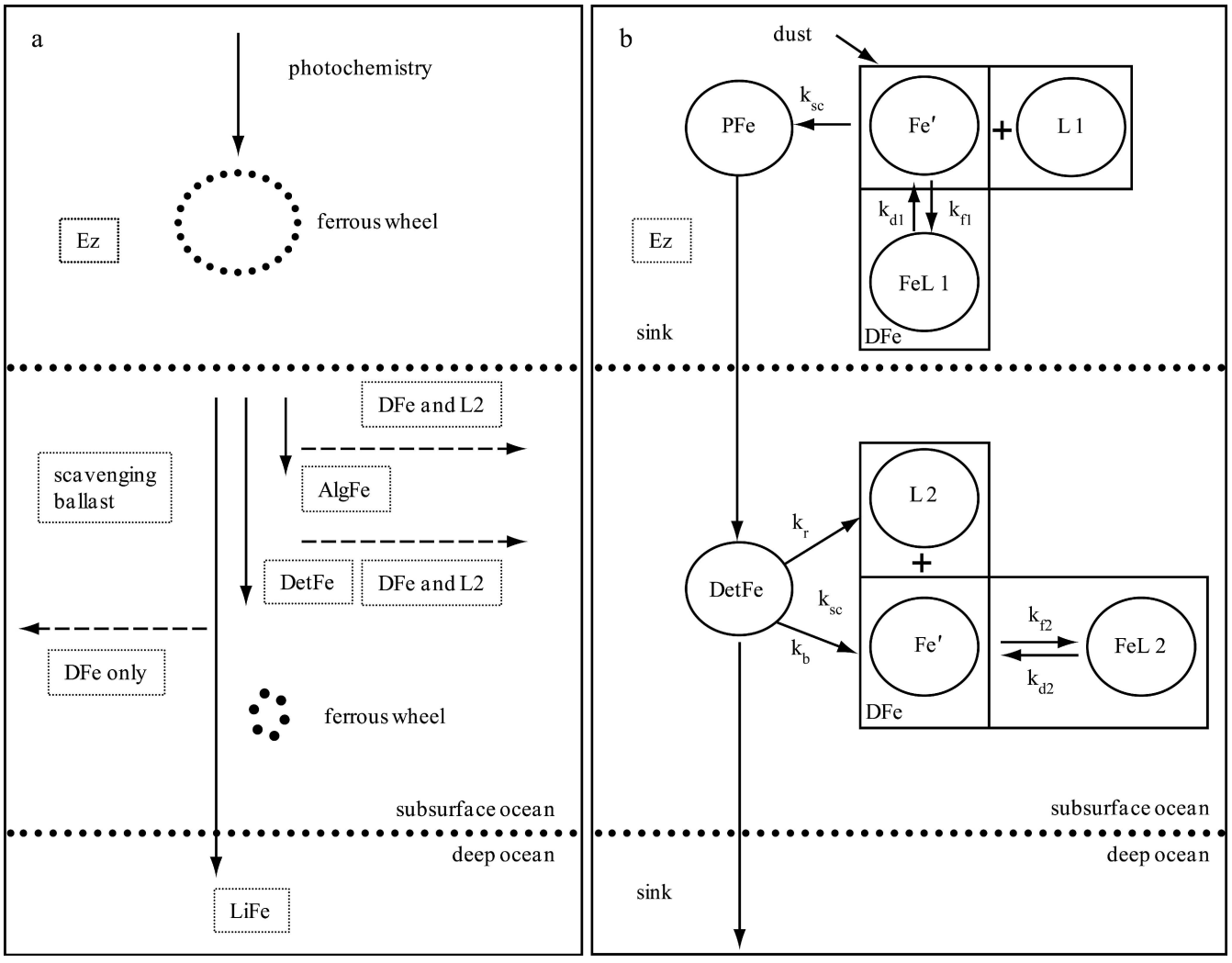

Fig. 8. (a) Schematic of the different roles lithogenic (LiFe), detrital (DetFe) and algal (AlgFe) PFe play in the iron biogeochemical cycle. The length of the vertical arrows denotes the relative remineralization length scales for each component. The dashed arrows denote the release of weak iron-binding ligands and/or DFe. Ez denotes the euphotic zone, and the subsurface ocean is defined here from the base of the Ez to 500-m depth. The different diameters of the ferrous wheels indicates the much faster rate of iron mobilization in surface waters relative to subsurface waters observed in our study. Although LiFe dominated the PFe inventory and downward fluxes at most ocean sites examined in this study, the remineralization of AlgFe and DetFe and the concurrent release of L2 may play a key role in maintaining DFe in the subsurface ocean. In contrast, LiFe may act to primarily scavenge DFe and more rapidly remove DetFe and AlgFe via mineral ballasting. The ratio of LiFe : DetFe : AlgFe for different ocean regions may set the relationship between retaining DFe and removing it from the subsurface ocean. (b) A schematic illustrating how our findings on the current release of weak iron-binding ligands and DFe could be incorporated into a more detailed model of ligand dynamics. In the upper ocean, we have redrawn the complexation model presented by Parekh et al. (2004). The original model parameterized the complexation of Fe′ with one ligand class, and the scavenging of Fe′ to PFe (solid arrows). Based on our results, we propose that the original model, with only one strong ligand L1, is relevant only for the surface mixed layer and that for the subsurface ocean, where L1 is absent, a second set of model parameters is required to take into account the release of Fe′ and a weaker ligand L2 from DetFe. L1 and L2 denote the strong and weaker ligand, with L2 being the product of remineralization. $-k_{sc}$ is the scavenging rate; k_b is the desorption rate of Fe′; k_r is the release rate of L2 from (DetFe); k_{fn} (k_{dn}) is the formation (dissociation) rate of each ligand class with Fe′; k_{f1} and k_{f2} are the formation rates of FeL1 and FeL2; and k_{d1} (k_{d2}) are the respective dissociation rates.

trophic bacteria do colonize phytoplankton cells and facilitate movement of iron from larger to smaller particles. However, the removal of micrograzers can slow the pelagic ferrous wheel. The remineralization of iron from sinking particles at depth releases both DFe and weak-binding ligands, with more of the latter than the former. Although important, the rate of subsurface remineralization is slow relative to that within the surface mixed layer (Fig. 8a).

Why does the recycling and remineralization of PFe decrease with depth? Two major differences between the surface and subsurface ocean are the transition from photic to aphotic conditions and the marked decrease in the abundances of microbial populations. Although microzoo-

plankton colonize settling particles and graze on bacteria attached to those particles (Kiørboe 2000), there is a marked decrease in both bacterial and bacterivore abundances with depth (Boyd et al. 1999; Ploug and Grossart 2000). Little is known about the relative decrease in these prey vs. predator abundances with depth. This decrease in the biota associated with settling particles might be best expressed as microbial biomass per unit PFe, and ideally as bacterial vs. bacterivore biomass per unit PFe, on attached particles.

The transition from sunlit waters to darkness decouples the siderophore–photochemical linkage that is reported to play an important role in the dissolution of lithogenic PFe (Borer et al. 2005). It will also halt the photodissolution of algal detritus (Mayer et al. 2009) and reduce recycling of elements such as iron. At sites such as BATS, where the flux is dominated by lithogenic PFe, decoupling this photochemistry–siderophore mechanism may result in the marked decrease in the mobilization of PFe between surface and subsurface waters. In contrast, at sites where detrital PFe dominates, such as KEOPS (Sarthou et al. 2008), it may be a combination of both this decoupling and also the rapid decrease in the abundance of attached microbial biota that slows the release of iron in subsurface waters. We have represented this transition with depth from high to low remineralization rates with large and small ferrous wheels in our conceptual model (Fig. 8a).

From evidence in our study and from datasets such as Frew et al. (2006), it appears that a major distinction between the algal, detrital, and lithogenic PFe that make up the bulk downward flux is the differences in their rates of decrease. Hence, in Fig. 8a we have represented their different remineralization length scales by vertical arrows. In our conceptual model, a high proportion of algal PFe is probably released as DFe and iron-binding ligands (in excess of DFe) in the 50-m stratum below the mixed layer (denoted by dashed horizontal arrows in Fig. 8a). In contrast, detrital PFe has a longer remineralization length scale and will likely release DFe and iron-binding ligands over a greater depth range. Lithogenic PFe probably releases a relatively small proportion of DFe with depth (around 10% based on the data in Frew et al. 2006) and importantly may not concurrently release iron-binding ligands. Hence, its biogeochemical roles may be mainly as a scavenging agent (Whitfield and Turner 1987) and as a ballasting substance (Armstrong et al. 2002) to remove detrital and algal PFe and recently released DFe (Fig. 8a).

Settling particles are complex heterogeneous structures (Lampitt et al. 1993) that can have all three PFe components present. In regions where one PFe form dominates, its biogeochemical role may be more readily elucidated. For example, BATS is dominated by lithogenic PFe, which from our simulations is the main source of DFe release. If the PFe flux is observed to act primarily as a ballast carrier and/or scavenger at this site, this would support our idea of no significant or concurrent release of weak ligands. Despite these uncertainties, our field experiments strongly suggest the need to incorporate subsurface ligand dynamics into iron biogeochemical models. We have attempted to illustrate this linkage in Fig. 8b by using a conceptual approach combining our findings on weak iron binding with the ligand dynamics model of Parekh et al. (2004). The interplay between the concurrent release of ligands, iron dissolution, and scavenging requires further experimental work and associated model simulations to develop further this conceptual model of the iron biogeochemical cycle in the open ocean.

Acknowledgments

We thank the officers, scientists, and crew of the R/V *Aurora Australis*, and voyage leaders Brian Griffiths and Simon Wright. Data from unpublished manuscripts were kindly provided by Imojen Pearce, Isabelle Dumont, and Simon Wright. We are grateful to Phoebe Lam for supplying mesopelagic particulate samples. P.W.B. was funded by the New Zealand Foundation for Research and Technology though the Coasts and Oceans Outcome Based Investment program. We are grateful for valuable comments from two reviewers and an associate editor that helped improve this manuscript.

References

Armstrong, R. A., C. Lee, J. I. Hedges, S. Honjo, and S. G. Wakeham. 2002. A new, mechanistic model for organic carbon fluxes in the ocean based on the quantitative association of POC with ballast minerals. Deep-Sea Res. II **49:** 219–236, doi:10.1016/S0967-0645(01)00101-1

Barbeau, K. 2006. Photochemistry of organic iron (III) complexing ligands in oceanic systems. Photochem. Photobiol. **82:** 1505–1516.

———, E. B. Kujawinski, and J. W. Moffett. 2001a. Remineralization and recycling of iron, thorium and organic carbon by heterotrophic marine protists in culture. Aquat. Microb. Ecol. **24:** 69–81, doi:10.3354/ame024069

———, J. W. Moffett, D. A. Caron, P. L. Croot, and D. L. Erdner. 1996. Role of protozoan grazing in relieving iron limitation of phytoplankton. Nature **380:** 61–64, doi:10.1038/380061a0

———, E. L. Rue, K. W. Bruland, and A. Butler. 2001b. Photochemical cycling of iron in the surface ocean mediated by microbial iron(III)-binding ligands. Nature **413:** 409–413, doi:10.1038/35096545

Bergquist, B. A., and E. A. Boyle. 2006. Dissolved iron in the tropical and subtropical Atlantic Ocean. Global Biogeochem. Cycles **20:** GB1015, doi:10.1029/2005GB002505

Bidle, K. D., and F. Azam. 1999. Accelerated dissolution of diatom silica by marine bacterial assemblages. Nature **397:** 508–512, doi:10.1038/17351

———, M. Manganelli, and F. Azam. 2002. Regulation of oceanic silicon and carbon preservation by temperature control on bacteria. Science **298:** 1980–1984, doi:10.1126/science.1076076

Borer, P. M., B. Sulzberger, P. Reichard, and S. M. Kraemer. 2005. Effect of siderophores on the light-induced dissolution of colloidal iron(III) (hydr)oxides. Mar. Chem. **93:** 179–193, doi:10.1016/j.marchem.2004.08.006

Bowie, A. R., and others. 2009. Different processes drive biogeochemical iron budgets in the subantarctic and polar Southern Ocean south of Australia during summer. Global Biogeochem. Cycles **23:** GB4034, doi:10.1029/2009GB003500

Boyd, P. W. 2004. Ironing out algal issues in the Southern Ocean. Science **304:** 396–397, doi:10.1126/science.1092677

———, and others. 1999. Transformations of biogenic particulates from the pelagic to the deep ocean realm. Deep-Sea Res. II **46:** 2761–2792, doi:10.1016/S0967-0645(99)00083-1

———, AND OTHERS. 2005. FeCycle: Attempting an iron biogeochemical budget from a mesoscale SF_6 tracer experiment in unperturbed low iron waters. Global Biogeochem. Cycles **19:** GB4S20, doi:10.1029/2005GB002494

BOYLE, E. 1997. What controls dissolved iron concentrations in the world ocean? A comment. Mar. Chem. **57:** 163–167, doi:10.1016/S0304-4203(97)00044-3

BRULAND, K. W., J. R. DONAT, AND D. A. HUTCHINS. 1991. Interactive influences of bioactive trace metals on biological production in oceanic waters. Limnol. Oceanogr. **36:** 1555–1577.

CHO, J.-C., AND OTHERS. 2007. Polyphyletic photosynthetic reaction centre genes in oligotrophic marine *Gammaproteobacteria*. Environ. Microbiol. **9:** 1456–1463, doi:10.1111/j.1462-2920.2007.01264.x

CROOT, P. L., AND M. JOHANSSON. 2000. Determination of iron speciation by cathodic stripping voltammetry in seawater using the competing ligand 2-(2-thiazolylazo)-p-cresol (TAC). Electroanalysis **12:** 565–576, doi:10.1002/(SICI)1521-4109(200005)12:8<565::AID-ELAN565>3.0.CO;2-L

DUCE, R. A., AND N. W. TINDALE. 1991. Atmospheric transport of iron and its deposition in the ocean. Limnol. Oceanogr. **36:** 1715–1726.

FREW, R. D., AND OTHERS. 2006. Particulate iron dynamics during FeCycle in subantarctic waters southeast of New Zealand. Global Biogeochem. Cycles **20:** GB1S93, doi:10.1029/2005GB002558

GERRINGA, L. J. A., P. M. J. HERMAN, AND T. C. W. POORTVLIET. 1995. Comparison of the linear Van den Berg/Ruzic transformation and a non-linear fit of the Langmuir isotherm applied to Cu speciation data in the estuarine environment. Mar. Chem. **48:** 131–142, doi:10.1016/0304-4203(94)00041-B

GNANADESIKAN, A., J. SARMIENTO, AND R. SLATER. 2003. Effects of patchy ocean fertilization on atmospheric carbon dioxide and biological production. Global Biogeochem. Cycles **17:** 1050, doi:10.1029/2002GB001940

HUANG, S., AND M. CONTE. 2009. Source/process apportionment of major and trace elements in sinking particles in the Sargasso Sea. Geochim. Cosmochim. Acta **73:** 65–90, doi:10.1016/j.gca.2008.08.023

HUNTER, K. A., AND P. W. BOYD. 2007. Iron-binding ligands and their role in the ocean biogeochemistry of iron. Environ. Chem. **4:** 221–232, doi:10.1071/EN07012

HUTCHINS, D. A., AND K. W. BRULAND. 1994. Grazer-mediated regeneration and assimilation of Fe, Zn and Mn from planktonic prey. Mar. Ecol. Prog. Ser. **110:** 259–269, doi:10.3354/meps110259

———, A. E. WITTER, A. BUTLER, AND G. W. LUTHER. 1999. Competition among marine phytoplankton for different chelated iron species. Nature **400:** 858–861, doi:10.1038/23680

IBISANMI, E. B., S. G. SANDER, P. W. BOYD, A. R. BOWIE, AND K. A. HUNTER. In press. Vertical distributions of Iron-(III) complexing ligands in the Southern Ocean. Deep-Sea Res.

JOHNSON, K. S., R. M. GORDON, AND K. H. COALE. 1997. What controls dissolved iron concentrations in the world ocean? Mar. Chem. **57:** 137–161, doi:10.1016/S0304-4203(97)00043-1

KIØRBOE, T. 2000. Colonization of marine snow aggregates by invertebrate zooplankton: Abundance, scaling and possible role. Limnol. Oceanogr. **45:** 479–484.

KIRCHMAN, D. L. 1996. Microbial ferrous wheel. Nature **383:** 303–304, doi:10.1038/383303a0

LAGLERA, L. M., AND C. M. G. VAN DEN BERG. 2009. Evidence for geochemical control of iron by humic substances in seawater. Limnol. Oceanogr. **54:** 610–619.

LAMBORG, C. H., K. O. BUESSELER, AND P. J. LAM. 2008. Sinking fluxes of minor and trace elements in the North Pacific Ocean measured during the VERTIGO program. Deep-Sea Res. II **55:** 1564–1577, doi:10.1016/j.dsr2.2008.04.012

LAMPITT, R. S., K. F. WISHNER, C. M. TURLEY, AND M. V. ANGEL. 1993. Marine snow studies in the Northeast Atlantic Ocean: Distribution, composition and role as a food source for migrating plankton. Mar. Biol. **116:** 689–702, doi:10.1007/BF00355486

MCKAY, R. M. L., AND OTHERS. 2005. Impact of phytoplankton on the biogeochemical cycling of iron in subantarctic waters southeast of New Zealand during FeCycle. Global Biogeochem. Cycles **19:** GB4S24, doi:10.1029/2005GB002482

MALDONADO, M. T., AND N. M. PRICE. 1999. Utilization of iron bound to strong organic ligands by plankton communities in the subarctic Pacific Ocean. Deep-Sea Res. II **46:** 2447–2473, doi:10.1016/S0967-0645(99)00071-5

MARTIN, J. H. 1990. Glacial-interglacial CO_2 change: The iron hypothesis. Paleoceanography **5:** 1–13, doi:10.1029/PA005i001p00001

———, S. E. FITZWATER, R. M. GORDON, C. N. HUNTER, AND S. J. TANNER. 1994. Iron, primary production and carbon-nitrogen flux studies during the JGOFS North Atlantic bloom experiment. Deep-Sea Res. II **40:** 115–134, doi:10.1016/0967-0645(93)90009-C

———, G. A. KNAUER, D. M. KARL, AND W. W. BROENKOW. 1987. VERTEX: Carbon cycling in the northeast Pacific. Deep-Sea Res. **34:** 267–285.

MAWJI, E., AND OTHERS. 2008. Hydroxamate siderophores: Occurrence and importance in the Atlantic Ocean. Environ. Sci. Technol. **42:** 8675–8680, doi:10.1021/es801884r

MAYER, L. M., L. L. SCHICK, K. R. HARDY, AND M. L. ESTAPA. 2009. Photodissolution and other photochemical changes upon irradiation of algal detritus. Limnol. Oceanogr. **54:** 1688–1698.

MOFFETT, J. W. 2002. Transformations among different forms of iron in the ocean, p. 343–373. *In* D. R. Turner and K. A. Hunter [eds.], Iron chemistry. Wiley.

MOORE, J. K., AND O. BRAUCHER. 2008. Sedimentary and mineral dust sources of dissolved iron to the world ocean. Biogeosciences **5:** 631–656.

MOREL, F. M. M., AND N. M. PRICE. 2003. The biogeochemical cycles of trace metals in the oceans. Science **300:** 944–947, doi:10.1126/science.1083545

PAREKH, P., M. J. FOLLOWS, AND E. BOYLE. 2004. Modeling the global ocean iron cycle. Global Biogeochem. Cycles **18:** GB1002, doi:10.1029/2003GB002061

PLOUG, H., AND H. P. GROSSART. 2000. Bacterial growth and grazing on diatom aggregates: Respiratory carbon turnover as a function of aggregate size and sinking velocity. Limnol. Oceanogr. **45:** 1467–1475.

RUE, E. L., AND K. W. BRULAND. 1995. Complexation of iron(III) by natural organic-ligands in the Central North Pacific as determined by a new competitive ligand equilibration adsorptive cathodic stripping voltammetric method. Mar. Chem. **50:** 117–138, doi:10.1016/0304-4203(95)00031-L

———, AND ———. 1997. The role of organic complexation on ambient iron chemistry in the equatorial Pacific Ocean and the response of a mesoscale iron addition experiment. Limnol. Oceanogr. **42:** 901–910.

SARTHOU, G., D. VINCENT, U. CHRISTAKI, I. OBERNOSTER, K. R. TIMMERMANS, AND C. P. D. BRUSSARD. 2008. The fate of biogenic iron during a phytoplankton bloom induced by natural fertilisation: Impact of copepod grazing. Deep Sea Res. II **55:** 734–752, doi:10.1016/j.dsr2.2007.12.033

Stanley, R. H. R., K. O. Buesseler, S. J. Manganini, D. K. Steinberg, and J. R. Valdes. 2004. A comparison of major and minor elemental fluxes collected in neutrally buoyant and surface-tethered sediment traps. Deep-Sea Res. I **51:** 1387–1395.

Strzepek, R. F., and P. J. Harrison. 2004. Photosynthetic architecture differs in coastal and oceanic diatoms. Nature **431:** 689–692, doi:10.1038/nature02954

———, M. T. Maldonado, J. L. Higgins, J. Hall, K. Safi, S. W. Wilhelm, and P. W. Boyd. 2005. Spinning the "ferrous wheel": The importance of the microbial community in an iron budget during the FeCycle experiment. Global Biogeochem. Cycles **19:** GB4S26, doi:10.1029/2005GB002490

Sunda, W. G., and S. A. Huntsman. 1995. Iron uptake and growth limitation in oceanic and coastal phytoplankton. Mar. Chem. **50:** 189–206, doi:10.1016/0304-4203(95)00035-P

Taylor, A. H., R. J. Geider, and F. J. H. Gilbert. 1997. Seasonal and latitudinal dependencies of phytoplankton carbon-to-chlorophyll a ratios: Results of a modeling study. Mar. Ecol. Prog. Ser. **152:** 51–66, doi:10.3354/meps152051

Trull, T. W., S. G. Bray, K. O. Buesseler, C. H. Lamborg, S. Manganini, C. Moy, and J. Valdes. 2008. In situ measurement of mesopelagic particle sinking rates and the control of carbon transfer to the ocean interior during the Vertical Flux in the Global Ocean (VERTIGO) voyages in the North Pacific. Deep-Sea Res. II **55:** 1684–1695, doi:10.1016/j.dsr2.2008.04.021

Twiss, M. R., and P. G. C. Campbell. 1995. Regeneration of trace metals from picoplankton by nanoflagellate grazing. Limnol. Oceanogr. **40:** 1418–1429.

Whitfield, M., and D. R. Turner. 1987. The role of particles in regulating the composition of seawater, p. 457–493. *In* W. Stumm [ed.], Aquatic surface chemistry. Wiley.

Associate editor: Mikhail V. Zubkov

Received: 03 August 2009
Accepted: 02 February 2010
Amended: 03 February 2010